An Effective Scale-Aware Edge-Smoothing Weighting Constraint-Based Weighted Guided Image Filter for Single Image Dehazing

Sumit Kr. Yadav[1] · Kishor Sarawadekar[1] iD

© The Author(s), under exclusive licence to Springer Science+Business Media, LLC, part of Springer Nature 2023

Abstract

This paper proposes a new effective scale-aware edge-smoothing weighting constraint-based weighted guided image filter (ESAESWC-WGIF) for single image dehazing. Edge-weighting constraint incorporated in this method is multi-scale and less sensitive to regularization parameter. It removes halo artifacts and over-smoothing strongly and preserves edge information in both flat and sharp regions more accurately than the guided image filter (GIF) and weighted guided image filter (WGIF). There are three main steps in the proposed method: In the first step, dark channel prior method is applied to hazy input image to estimate atmospheric map and transmission map. In the next step, we refine the initial transmission map using the proposed ESAESWC-WGIF. It removes halo artifacts, over-smoothing effect strongly and preserves edge information in both flat and sharp regions. In the final step, the haze-free image is recovered from the scene radiance. About 3200 images from Fattal, NYU2, D-HAZY, Haze-RD, and O-Haze datasets are used to compare the performance of the proposed filter with the existing image dehazing methods. Experimental results prove that the proposed method is independent of the nature of the input image. Moreover, it produces better visual quality. It is noteworthy that the proposed method is faster than the existing methods for a given resolution of images.

Keywords Dark channel prior · Edge preservation · Guided image filter · Transmission map · Haze removal

✉ Kishor Sarawadekar
skishor.ece@iitbhu.ac.in

Sumit Kr. Yadav
sumitkryadav.rs.ece17@iitbhu.ac.in

1 Department of Electronics Engineering, Indian Institute of Technology (BHU), Varanasi, Varanasi, U.P 221005, India

Birkhäuser

1 Introduction

The visual quality of the outdoor images is seriously degraded due to hazy weather. Haze, fog, water droplets, suspended particles, etc., are different conditions of bad weather. The outdoor images captured under this situation have poor color, contrast, and visibility [7, 33, 38]. The reason for the formation of these types of turbid mediums is scattering and absorption of light by different aerosols present in the atmosphere [22, 36]. Image dehazing is extremely desired in computational photography, image processing, and computer vision [10, 32]. It can significantly reduce color and visibility and increase the contrast of hazy images. To improve the performance of hazy images, many algorithms have been proposed in different applications of computational photography, computer vision, and image processing. Due to unknown distances from the camera to scene points as well as unknown airlight, it is tough to remove haze from the input image. Several methods have been developed to remove haze. Tan et al. proposed a local contrast optimization-based haze removal method [38]. However, experimental results produce color distortion and halo artifacts. He et al. proposed a novel dark channel prior (DCP) [12] method for single image dehazing. However, this method is not applicable to large sky regions and halo artifacts, as well as color distortions, persist in both flat and sharp regions. To reduce halo artifacts, different edge-preserving image filters have been proposed [13, 23, 26, 39, 44]. Bilateral filters and their improved versions are widely used in image processing [39, 44]. But, the pixels cannot maintain consistency near the edges, and hence, edge information is not preserved appropriately. Further, He et al. developed local linear model-based guided image filter (GIF) [13] to overcome the drawback of bilateral filter [39]. It is a good edge-preserving filter. Here, the contents of the guided image or different images are considered as filter input. It has wide applications in image processing like detail enhancement, reduction in edge smoothing, image feathering, denoising, etc. However, halo artifacts and over smoothing persist in the sharp regions. Further, a weighted guided image filter (WGIF) [26] was proposed to reduce the halo artifacts by introducing an edge-aware weighting factor in the existing GIF [13]. But, due to the local linear model, it is unable to preserve edge information in the sharp regions. In this paper, we propose an effective scale-aware edge-smoothing weighting constraint-based weighted guided image filter (ESAESWC-WGIF) for single image dehazing. The main contributions of this work are summarized as

- In this paper, we propose a new effective scale-aware edge-smoothing weighting constraint-based weighted guided image filter (ESAESWC-WGIF) for single image dehazing.
- The proposed edge-smoothing weighting is a multi-scale-based local linear filter, and it is less sensitive to the regularization parameter than the GIF, WGIF, GGIF, and EGIF methods.
- This filter is proposed by incorporating of ESAESWC into the cost function of GIF.
- It is an excellent edge-preserving filter and removes halo artifacts and over-smoothing strongly in both flat and sharp regions.

- To analyze the effectiveness of the proposed method, we have evaluated PSNR, SSIM, FADE, and CIEDE2000 metrics for different datasets, viz. Fattal, NYU2, D-HAZY, Haze-RD, and O-Haze datasets. Experimental results prove that the proposed method achieves favorable performance against the existing haze removal methods.

The remaining part of this paper is framed as follows. In Sect. 2, we shortly review the related works. Section 3 covers the preliminary work essential for understanding the GIF and related edge-preserving filtering concept. The proposed dehaze algorithm is detailed in Sect. 4. Experimental outcomes are discussed in Sect. 5, and Sect. 6 concludes the paper.

2 Related Work

This work is related to prior-based, edge-preserving filter-based, and deep-learning-based haze removal methods.

2.1 Prior-Based Haze Removal Methods

Various prior-based haze removal methods are in existence. The prior-based well-known haze removal methods are DCP [12], CAP [48], DSPP [14], CEP [4], BDPK [19], IDGCP [20], SIPSID [29], and IDBP [21]. He et al. proposed a dark channel prior (DCP) [12] method for single image dehazing. In DCP, dark channel is defined as at least one color channel has very low intensity in the non-sky regions. However, it fails when bright objects are present in the scene. Moreover, it is computationally inefficient due to soft matting. It generates halo artifacts and color distortions at depth discontinuity. Zhu et al. proposed a color attenuation prior (CAP) method in [48] for single image dehazing. Here, a linear model-based supervised learning method is used to evaluate the depth information of the input hazy image. Next, He et al. proposed an optimal transmission map-based difference structure preservation prior [14] method for single image dehazing. This method used an image patch as a sparse linear combination of the elements to obtain accurate transmission map. Next, Bui et al. proposed a color ellipsoid prior [4] method for single image dehazing. This method used a color ellipsoid geometry to calculate the transmission map which increases contrast of the restored image pixels, while preventing over-saturated pixels. In this prior, Ju et al. proposed an adaptive and more reliable atmospheric scattering model (RASM)-based algorithm known as Bayesian dehazing algorithm (BDPK) [19]. This method directly converts the image dehazing process into an optimization function using Bayesian theory and prior knowledge and restore the scene albedo with an alternating minimizing technique (AMT). Next, an effective gamma correction prior (GCP)-based atmospheric scattering model (ASM) is proposed in [20] for image dehazing. In this model, first an input image is transformed into a virtual image and it is combined with an input image to calculate scene depth of image dehazing. Next, Lu et al. proposed a saturation-based iterative dark channel prior (IDCP) [29] method for single image dehazing. In IDCP, dark channel is reformulated in saturation and brightness terms

and estimates the transmission map without computing the dark channel. In [21], Lu et al. proposed a novel blended prior model for single image dehazing (IDBP). This method has two modules such as atmospheric light estimation (ALE) and a multiple prior constraint (MPC) to remove haze from input image. The prior-based methods remove haze efficiently. However, they fail to preserve edge information in the sharp regions and halo artifacts are observed in the dehazed image.

2.2 Edge-Preserving Filtering-Based Haze Removal Methods

Halo artifact is a major problem in haze removal algorithms. Therefore, He et al. developed a novel guided image filter (GIF) [13] for single image dehazing. In this algorithm, a local linear model is used to represent iterated output with the help of a guided image. This method reduces the halo artifacts and preserves the edge information more accurately. But, GIF [13] fails to preserve edge information in sharp regions due to local linear model and large computational complexity. Next, Li et al. proposed a weighted guided image filter (WGIF) [26] for image dehazing. It removes halo artifacts strongly and preserves the edge information more accurately in the sharp regions than the GIF [13]. However, due to local linear model and fixed regularization parameter, over-smoothing takes place in the sharp regions. Next, Kou et al. proposed a multi-scale edge-aware weighting-based gradient domain guided image filter (GGIF) [23] to avoid over smooth images in flat regions and reduce halo artifacts more strongly than WGIF [26]. But, over-smoothing in the sharp regions increases with an increase in the regularization parameter. In EGIF [28], the average of local variances for all pixels is incorporated in the cost function of GIF [13]. It removes halo artifacts effectively and preserves edge information more precisely than GIF [13], WGIF [26], GGIF [23] methods. However, it also over smooth images in the sharp regions depending on the value of the regularization parameter. Next, Geethu et al. proposed a weighted guided image filter for image dehazing [11]. In [15], Hong et al. developed weighted guided image filtering-based a local stereo matching algorithm to improve scene depth of hazy image. Chen et al. proposed a weighted aggregation model using guided image filter for single image dehazing in [6]. In [16], Hong et al. proposed a fast guided image filtering-based real-time local stereo matching algorithm for image dehazing.

2.3 Deep-Learning-Based Haze Removal Methods

With the popularity of convolutional neural network (CNN), many deep-learning-based haze removal methods such as DehazeNet [5], AOD-Net [24], Proximal dehazeNet[43], PDR-Net[25], FFA-Net[34], and RefineDNet [47] have been proposed for image dehazing. In [5], Cai et al. proposed a trainable deep learning architecture called DehazeNet to estimate transmission map and then remove haze by atmospheric scattering model (ATSM). In [5], a nonlinear activation function called Bilateral Rectified Linear Unit (BReLU) is proposed to restore the haze-free image more accurately. Next, Aod et al. proposed an end-to-end CNN-based deep learning model called AOD-Net [24] to remove haze. It is designed by re-formulating ATSM and directly generates

the haze-free image through a lightweight CNN. Yang et al. [43] presented a CNN-based deep architecture for single image dehazing by learning dark channel prior and transmission map. This method used a proximal learning-based iterative deep learning algorithm called proximal DehazeNet for single image dehazing. Next, Li et al. proposed a deep CNN for single image dehazing named PDR-Net [25]. Here, a perception-driven image dehazing sub-network is designed for single image dehazing. The refined sub-network improves the contrast and visual quality of the dehazed image. Next, Qin et al. proposed an end-to-end feature fusion attention network (FFA-Net) [34] which combines the channel attention and pixel attention approach to directly recover the haze-free image. This method performs outstanding in case of thick haze and rich texture details. Zhao et al. proposed a two stage weakly supervised framework named RefineDNet [47] for single image dehazing. In [47], first prior-based DCP is used to recovered the visibility and then introduced generative adversarial network (GAN) to enhance the contrast and realness of the dehazed image. However, these methods are impractical and most of the models are trained on synthetic hazy datasets and often fail when tested on real hazy datasets. They require enormous computation and memory resources, especially with the increase in network depth.

3 Background

In GIF [13], the filtered output is linearly related to the guidance image, and it is expressed as

$$q_i = a_k I_i + b_k, \quad \forall i \in \omega_{\zeta_1}(k), \tag{1}$$

where I_i represents an input the guidance image and q_i represents its linear transform in window ω_{ζ_1} at ith pixel position with radius ζ_1 and (a_k, b_k) represent constant linear coefficients in window ω_{ζ_1} at pixel position kth.
The minimized cost function in window $\omega_{\zeta_1}(k)$ can be expressed as

$$E(a_k, b_k) = \sum_{i \in \omega_{\zeta_1}(k)} ((a_k I_i + b_k - p_i)^2 + \varepsilon a_k^2), \tag{2}$$

where p_i represents a filter input and ε represents a regularization parameter used to penalize large a_k. The cost function in Eq. (2) is a linear ridge regression model [8, 49], and its optimal solution is given in terms of linear coefficients (a_k, b_k) as

$$a_k = \frac{\frac{1}{|\omega|} \sum_{i \in \omega_{\zeta_1}(k)} I_i p_i - \mu_k \overline{p}_k}{\sigma_k^2 + \varepsilon}, \tag{3}$$

$$b_k = \overline{p}_k - a_k \mu_k. \tag{4}$$

where $|\omega|$ represents number of pixels, μ_k is mean, σ_k^2 is variance and $\overline{p}_k$ is average or mean of p in window $\omega_{\zeta_1}(k)$. The regularization parameter (ε) and variance σ_k^2 play a vital role in preserving edges in smooth and sharp regions. Specifically, ε should be
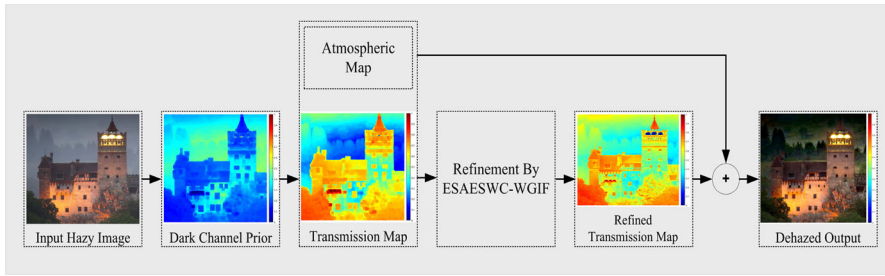
Fig. 1 The basic framework of the proposed haze removal method

larger than σ_k^2 to preserve edges in smooth regions and ε should be smaller than σ_k^2 to preserve edges in the sharp regions.

In order to keep the edge information more accurately than the GIF [13], a weighted guided image filter (WGIF) is proposed in [26]. In WGIF [26], local variance is replaced by a new edge-aware weighting $\Gamma_I(k)$, and it can be expressed as

$$\Gamma_I(k) = \frac{1}{N} \sum_{i=1}^{N} \frac{\sigma_{I,1}^2(k) + \lambda}{\sigma_{I,1}^2(i) + \lambda},$$ (5)

where N indicates the pixel number of the guidance image I and the parameter λ is a small constant and its value is selected by as $(0.001 \times M)^2$ with M being the dynamic intensity range of the image. $\sigma_{I,1}^2(k)$ and $\sigma_{I,1}^2(i)$ are the local variance of I in the windows ω_k and ω_i, respectively. The optimized cost function for WGIF [26] can be expressed as

$$E(a_k, b_k) = \sum_{i(x,y) \in \omega_{\zeta_1}(k)} \left\{ (a_k I_i + b_k - p_i)^2 + a_k^2 \frac{\varepsilon}{\Gamma_I(k)} \right\}.$$ (6)

The optimal value of a_k and b_k is obtained by the following expression:

$$a_k = \frac{\mu_{I*p,\zeta_1}(k) - \mu_{I,\zeta_1}(k)\mu_{p,\zeta_1}(k)}{\sigma_{I,\zeta_1}^2(k) + \frac{\varepsilon}{\Gamma_I(k)}},$$ (7)

$$b_k = \mu_{p,\zeta_1}(k) - a_k \mu_{I,\zeta_1}(k).$$ (8)

where μ_{I*p} represents the mean of $(I * p)$.

4 Proposed Method

In this paper, an effective scale-aware edge-smoothing weighting constraint-based weighted guided image filter (ESAESWC-WGIF) is proposed for single image dehazing. The basic framework of the proposed method is shown in Fig. 1. The proposed method has three main steps as follows: In the first step, the dark channel prior (DCP)

[12] method is used to compute the atmospheric and transmission maps accurately. In the second step, we refined the raw transmission map by ESAESWC-WGIF algorithm to remove halo artifacts, over smooth, and preserve edge information more accurately in both flat and sharp regions. Finally, we recovered the dehazed image from the scene radiance.

4.1 Dark Channel Prior (DCP)-Based Atmospheric Map and Transmission Map Estimation

The popular Koschmieder's law [18] is generally used to represent the haze formation. However, McCartney [30] improved Koschmieder's law by estimating the atmospheric map as well as transmission map more accurately. In this model, haze formation is represented by the following expression:

$$I(x) = J(x)t(x) + A(1 - t(x)), \qquad (9)$$

where x is pixel's position into the image, $I(x)$ is input hazy image, $J(x)$ is output dehaze image or scene radiance, $t(x)$ is the medium transmission map, and A is the global atmospheric light or map. In Eq. (9), the first term $J(x)t(x)$ and the second term $A(1 - t(x))$ are called direct attenuation and airlight, respectively.

The relation of medium transmission map $t(x)$ with the object's distance $d(x)$ can be expressed as

$$t(x) = \exp(1 - \beta d(x)) \le 1, \qquad (10)$$

where $0 \le d(x) \le \infty$ is the depth (distance) of scene point (pixel) from camera and β is the scattering coefficient related to the wavelength of light and it is exponentially attenuated with the scene depth $d(x)$. The single image haze removal result can be obtained by putting $t(x)$ and A value in Eq. (9).

According to dark channel prior (DCP) [12] method, J can be estimated after assuming some prior information. In DCP [12], dark pixel (lowest pixel) concept is used to calculate transmission map $t(x)$ and $A(x)$. In DCP [12], the atmospheric map A is estimated by selecting top 0.1% of brightest pixels in hazy image. For a given atmospheric map A, Eq. (9) can be modified as

$$\frac{I^c(x)}{A^c} = t(x)\frac{J^c(x)}{A^c} + 1 - t(x), \qquad (11)$$

where c denotes color channels (r, g, b). A^c and J^c represent the atmospheric map and dehaze image for color channel, respectively. Due to constant behavior of transmission map $t(x)$ in a local patch $\Omega(x)$, it is denoted by $\tilde{t}(x)$ [12]. Dark channel is computed after substituting the minimum operator on both sides of Eq. (11).

$$\min_{y \in \Omega(x)} \left(\min_{c \in \{r,g,b\}} \frac{I^c(y)}{A^c} \right) = \tilde{t}(x) \min_{y \in \Omega(x)} \left(\min_{c \in \{r,g,b\}} \frac{J^c(y)}{A^c} \right) + 1 - \tilde{t}(x). \qquad (12)$$

Algorithm 1 ESAESWC-WGIF for single image dehazing

Input: Input hazy image $I(x)$, Atmospheric map A, Transmission map $t(x)$, Refine transmission map $\tilde{t}(x)$, filtering input image $p(x)$, linear transform q_i, linear constants a_k, b_k.
1: Calculate Atmospheric map A and Transmission map $t(x)$ using DCP [12] by Eq. (9) and Eq. (10), respectively.
2: Calculate minimum cost function using proposed ESAESWC $\overline{\psi}_I(k)$ by Eq. (19).
3: Calculate optimized linear constants a_k, b_k by Eq. (28) and Eq. (24), respectively.
4: Calculate refined transmission map $\overline{t}(x)$ by Eq. (31)
5: Calculate mean values of linear constants $\overline{a}_k, \overline{b}_k$ by Eq. (32) and Eq. (33), respectively.
Output: Dehazed output image $J(x)$ is calculated by Eq. (34).

According to DCP [12], to restore the scene radiance J as haze-free image, the dark channel of the scene radiance should be zero, and it can be expressed as

$$J^{dark}(x) = \min_{y \in \Omega(x)} \left(\min_c \frac{J^c(y)}{A^c} \right) = 0, \tag{13}$$

where J^{dark} is a scene radiance for dark channel. Since A^c should always positive, Eq. (12) can be modified as

$$\min_{y \in \Omega(x)} \left(\min_c \frac{I^c(y)}{A^c} \right) = 1 - \tilde{t}(x). \tag{14}$$

After simplification, $\tilde{t}(x)$ can be expressed as

$$\tilde{t}(x) = 1 - \min_{y \in \Omega(x)} \left(\min_c \frac{I^c(y)}{A^c} \right), \tag{15}$$

We know that the DCP [12] method is not valid for large sky, sea, or white regions because the color of sky or ocean during haze is mostly similar to atmospheric map. Due to that, the transmission map becomes close to 0 [12, 41, 42]. Finally, the transmission map can be expressed as

$$\tilde{t}(x) = 1 - w \min_{y \in \Omega(x)} \left(\min_c \frac{I^c(y)}{A^c} \right). \tag{16}$$

Here, a constant parameter w $(0 < w \leq 1)$ is used to retain a very limited amount of haze for distant objects.

4.2 Effective Scale-Aware Edge-Smoothing Weighting Constraint-Based Weighted Guided Image Filter (ESAESWC-WGIF)

In this paper, a new multi-scale edge-aware weighting constraint-based an effective weighted guided image filter is proposed for single image dehazing. The new multi-scale edge-weighting constraint is incorporated in the cost function of the GIF [13].

The proposed method removes halo artifacts and over-smoothing effect strongly and preserves edge information appropriately in both flat and sharp regions.

In GIF [13], the regularization parameter ε is identical for all local windows and due to that it is unable to preserve sharp edges appropriately and hence halo artifacts exhibit near edges in the output images. To overcome this problem, a single scale edge-aware weighting was initially proposed in weighted guided image filter (WGIF) [26]. In this filter, a 3×3 window has been considered for every pixel while computing local variance and the regularization parameter ε is replaced with $\varepsilon \Gamma_I(k)$. It removes halo artifacts and preserves edge information more accurately than GIF. However, over-smoothing effect persists in the sharp regions due to single scale edge-aware weighting. In this paper, we are proposing a method to overcome this issue by introducing a new effective scale-aware edge-smoothing weighting constraint-based weighted guided image filter (ESAESWC-WGIF). It is multi-scale edge-aware weighting constraint which is defined using local variance of both 3×3 and $(2\zeta_1 + 1) \times (2\zeta_1 + 1)$ windows of each pixel in the guidance image I. The following expression can be used to express the average of local variances for all pixels:

$$\overline{\psi}_I(k) = \frac{\sigma_{I,1}(k)}{\overline{\sigma}^2}, \tag{17}$$

and $\overline{\sigma}^2$ is expressed as

$$\overline{\sigma}^2 = \frac{1}{N} \sum_{k=1}^{N} \sigma_{I,\zeta_1}^2(k). \tag{18}$$

where N indicates the pixel number of the guidance image I, $\sigma_I, 1(k)$ and $\sigma_{I,\zeta_1}^2(k)$ are the local variances of I in 3×3 windows and $(2\zeta_1 + 1) \times (2\zeta_1 + 1)$ windows of all pixels.

The minimum cost function for the proposed ESAESWC-WGIF can be expressed as

$$E(a_k, b_k) = \sum_{i(x,y) \in \omega_{\zeta_1}(k)} \left\{ (a_k I_i + b_k - p_i)^2 + a_k^2 \frac{\varepsilon}{\overline{\psi}_I(k)} \right\}. \tag{19}$$

The modified a_k value is calculated by the following expression:

$$a_k = \frac{\mu_{I*p,\zeta_1}(k) - \mu_{I,\zeta_1}(k)\mu_{p,\zeta_1}(k)}{\sigma_{I,\zeta_1}^2(k) + \frac{\varepsilon}{\overline{\psi}_I(k)}}, \tag{20}$$

and b_k is calculated as mentioned in Eq. (8). For better analysis, I and p can be assumed identical and it can be expressed after simplification as

$$\mu_{I*p,\zeta_1}(k) - \mu_{I,\zeta_1}(k)\mu_{p,\zeta_1}(k) = \sigma_{I,\zeta_1}^2(k) \tag{21}$$

and

$$\mu_{p,\zeta_1}(k) = \mu_{I,\zeta_1}(k). \tag{22}$$

After substituting Eqs. (21) and (22) in Eq. (20), we obtain

$$a_k = \frac{\sigma_{I,\zeta_1}^2(k)}{\sigma_{I,\zeta_1}^2(k) + \frac{\varepsilon}{\overline{\psi}_I(k)}}, \tag{23}$$

and

$$b_k = (1 - a_k)\mu_{I,\zeta_1}(k), \tag{24}$$

or it is simply written as

$$a_k = \frac{\sigma_{I,\zeta_1}^2(k)}{\sigma_{I,\zeta_1}^2(k) + \frac{\varepsilon}{\overline{\psi}_I(k)}}. \tag{25}$$

After dividing Eq. (25) by $\sigma_{I,\zeta_1}^2(k)$, we get

$$a_k = \frac{1}{1 + \varepsilon \frac{1}{\sigma_{I,\zeta_1}^2}(k)\overline{\psi}_I(k)}, \tag{26}$$

Substituting value of $\overline{\psi}_I(k)$ from (17) into (26)

$$a_k = \frac{1}{1 + \varepsilon \dfrac{1}{\left\{\sigma_{I,\zeta_1}^2(k)\right\} * \left\{\frac{\sigma_{I,1}(k)}{\overline{\sigma}^2}\right\}}} \tag{27}$$

$$a_k = \frac{1}{1 + \varepsilon \dfrac{\overline{\sigma}^2}{\sigma_{I,\zeta_1}^2(k) * \sigma_{I,1}(k)}}. \tag{28}$$

Finally, q_i is expressed as

$$q_i = \frac{1}{|\omega_{\zeta_1}(k)|} \sum_{k \in \omega_{\zeta_1}(k)} (a_k I_i + b_k), \tag{29}$$

$$q_i = (\overline{a}_i I_i + \overline{b}_i), \tag{30}$$

After obtaining linear constants a_k and b_k, the filtered output q_i is now the refined transmission map (refined filtered output). It can be expressed as

$$q_i = \overline{t}(x) = (\overline{a}_i I_i + \overline{b}_i), \tag{31}$$

where $\overline{a}_i$ and $\overline{b}_i$ terms in the above expression represent mean of a_k and b_k, respectively, in the corresponding window of all pixels, and it is computed as

$$\overline{a}_i = \frac{1}{|\omega_{\zeta_1}(k)|} \sum_{k \in \omega_{\zeta_1}(k)} a_k, \qquad (32)$$

$$\overline{b}_i = \frac{1}{|\omega_{\zeta_1}(k)|} \sum_{k \in \omega_{\zeta_1}(k)} b_k. \qquad (33)$$

In order to preserve edge information in sharp regions, a_k should be 1 and b_k close to 0, whereas for smooth regions a_k close to 0 and b_k become 1 [26]. Finally, the dehazed output image is calculated by following expression:

$$J(x) = \frac{I(x) - A}{\max(\overline{t}(x), t_0)} + A. \qquad (34)$$

where the value of t_0 is set to 0.1 [13] for avoiding noise amplification.

5 Experimental Results and Analysis

The proposed algorithm is experimented and evaluated using MATLAB R2018a on a PC with Intel (R) Core (TM) i7-6700 CPU @ 3.40 GHz of a 64-bit operating system with RAM-8GB. The performance of the proposed method is tested on natural hazy, non-hazy and synthetic images of different datasets, viz. Fattal's (580 images) [10], NYU2 (650 images) [37], D-HAZY (400 images) [1], Haze-RD (760 images) [46], and O-HAZE (810 images) [2] and the outcomes are compared with existing DCP [12] GIF [13], WGIF [26], GGIF [23], EGIF [28], DehazeNet [5], and RYF-Net [9] haze removal methods for effective analysis.

5.1 Qualitative Analysis

In this paper, the proposed method is tested on about 3200 images of hazy, non-hazy and synthetic images from Fattal [10], NYU2 [37], D-HAZY [1], Haze-RD [46], and O-HAZE [2] datasets and the outcomes are compared with 7 state-of-the-art haze removal methods, out of which DCP [12] is prior-based dehazing method, GIF [13], WGIF [26], GGIF [23], and EGIF [28] are four edge-preserving image dehazing filters, and DehazeNet [5] and RYF-Net [9] are two deep-learning-based image dehazing methods. The refined transmission map by GIF [13], WGIF [26], GGIF [23], EGIF [28] and the proposed method for input hazy building image [10] is shown in Fig. 2 . It is clear from Fig. 2 that the proposed method is refined the raw transmission map more accurately than the rest of the existing methods. It removes halo artifacts, over-smoothing, color distortion strongly and preserves edge information more precisely than the existing GIF [13], WGIF [26], GGIF [23], and EGIF [28] methods. Several hazy images from different datasets, viz. Fattal [10], NYU2 [37], D-HAZY [1], Haze-RD [46], and O-HAZE [2], are tested for better analysis of the proposed method, and
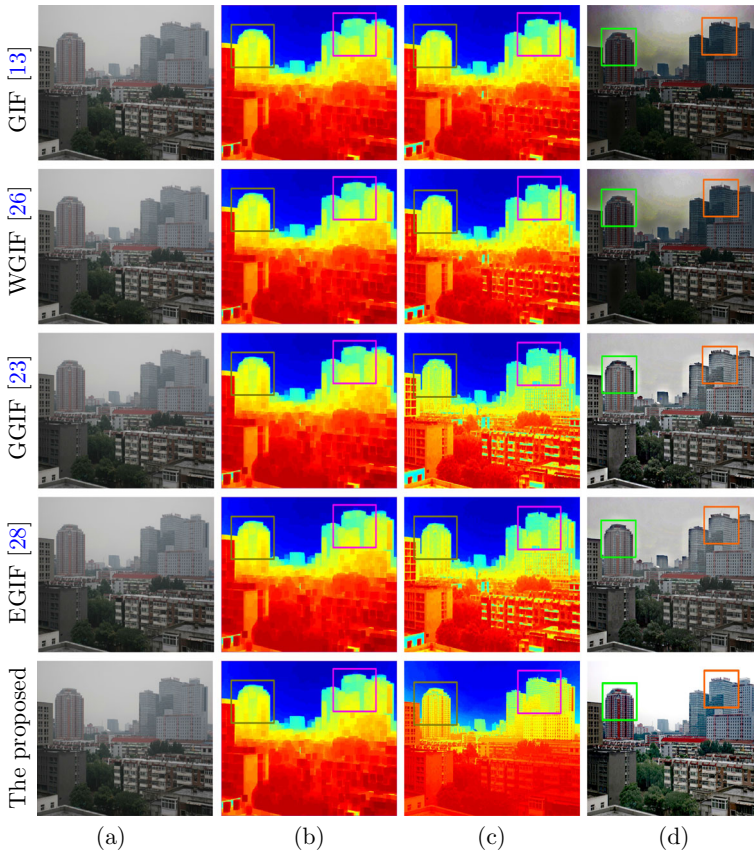
Fig. 2 Comparison of refined transmission maps of different edge-preserving filters. **a** Input hazy images [10], **b** DCP [12]-based transmission map, **c** refined transmission map by GIF [13], WGIF [26], GGIF [23], EGIF [28] and the proposed method **d** Dehazed output

their outcomes are compared with existing DCP [12], GIF [13], WGIF [26], GGIF [23], EGIF [28], DehazeNet [5], and RYF-Net [9] haze removal methods. The dehazed outcomes of DCP [12], GIF [13], WGIF [26], GGIF [23], EGIF [28], DehazeNet [5], and RYF-Net [9] and the proposed method are calculated for five benchmark hazy images [10] and presented in Figs. 3, 4, 5, 6, and 7, respectively, for effective visual comparison. It is clear from Figs. 3, 4, 5, 6, and 7 that the proposed method removes halo artifacts, over-smoothing strongly and preserves edge information more precisely in both flat and sharp regions than the existing DCP [12], GIF [13], WGIF [26], GGIF [23], EGIF [28], DehazeNet [5], and RYF-Net [9] methods.

5.2 Quantitative Analysis

The objective evaluation of the proposed filter is compared with the existing GIF [13], WGIF [26], GGIF [23], and EGIF [28] methods using an effective blind object
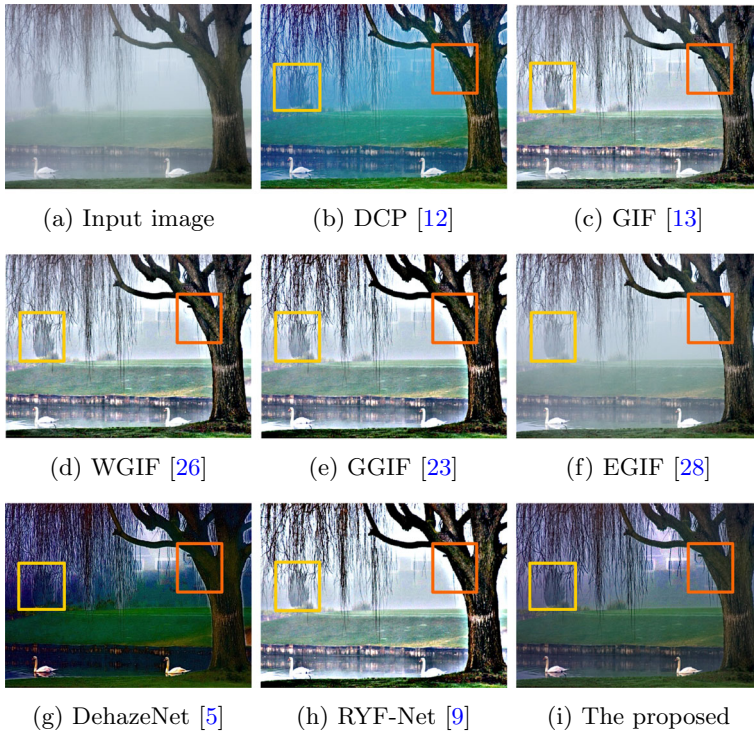
Fig. 3 Dehazed outcomes of different haze removal methods and the proposed method. **a** Input hazy image [10], **b** DCP [12], **c** GIF [13], **d** WGIF [26], **e** GGIF [23], **f** EGIF [28], **g** DehazeNet [5], **h** RYF-Net [9], **i** the proposed

Table 1 Objective evaluation on images in Fig. 3 by [31]

	GIF [13]	WGIF [26]	GGIF [23]	EGIF [28]	The proposed
Input	36.87	36.87	36.87	36.87	36.87
$\varepsilon = 0.001^2$	**39.64**	38.19	39.22	39.07	39.45
$\varepsilon = 0.05^2$	41.36	42.19	45.38	46.52	**46.85**
$\varepsilon = 0.1^2$	35.67	37.46	45.15	46.23	**46.72**
$\varepsilon = 0.4^2$	31.26	32.91	43.69	44.51	**46.57**
$\varepsilon = 0.8^2$	27.35	29.87	42.53	43.66	**46.19**

image quality metric [31]. Score of these filters are calculated for different values of the regularization parameter ε and their values are listed in Table 1. As we can seen clearly from Table 1 that the scores of GIF [13] and WGIF [26] initially increase and then decrease for large ε value. However, GGIF [23] and EGIF [28] both have higher scores than GIF [13] and WGIF [26] but they also generate lower scores for large ε values ($\varepsilon = 0.4^2, 0.8^2$), whereas the scores of the proposed method increase with the increase in ε and decrease slightly even for large ε values. In this paper, some performance

(a) Input image (b) DCP [12] (c) GIF [13]

(d) WGIF [26] (e) GGIF [23] (f) EGIF [28]

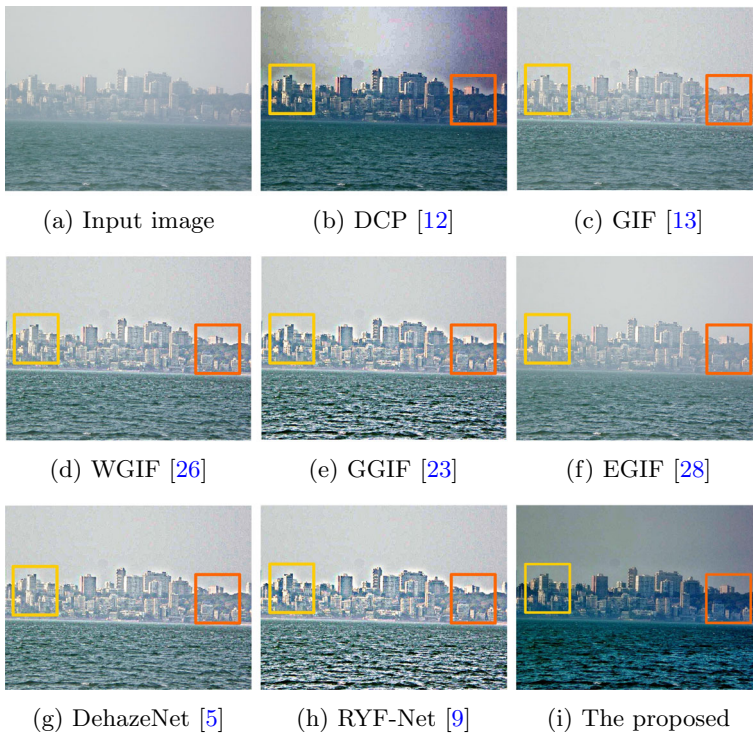(g) DehazeNet [5] (h) RYF-Net [9] (i) The proposed

Fig. 4 Dehazed outcomes of different haze removal methods and the proposed method. **a** Input hazy image [37], **b** DCP [12], **c** GIF [13], **d** WGIF [26], **e** GGIF [23], **f** EGIF [28], **g** DehazeNet [5], **h** RYF-Net [9], **i** the proposed

metrics such as peak signal-to-noise ratio (PSNR) [17], structural similarity index (SSIM) [40], fog aware density evaluator (FADE) [7], and CIEDE2000 [35] are used for effective assessment of the proposed method. The performance metrics of DCP [12], GIF [13], WGIF [26], GGIF [23], EGIF [28], DehazeNet [5], RYF-Net [9] and the proposed method are calculated for hazy images from Fattal [10], NYU2 [37], D-HAZY [1], Haze-RD [46], and O-HAZE [2] datasets, and their outcomes are furnished in Tables 2, 3, 4, 5, and 6, respectively. The blue bold faces in Tables 2, 3, 4, 5, and 6 indicate the best value.

5.2.1 Peak Signal-to-Noise Ratio (PSNR)

The higher peak signal-to-noise ratio (PSNR) [17] indicates better image restoration result. It is expressed as

$$PSNR = 10 * \log \left\{ \frac{f_{max}^2}{MSE} \right\}, \tag{35}$$

(a) Input image   (b) DCP [12]   (c) GIF [13]

(d) WGIF [26]   (e) GGIF [23]   (f) EGIF [28]

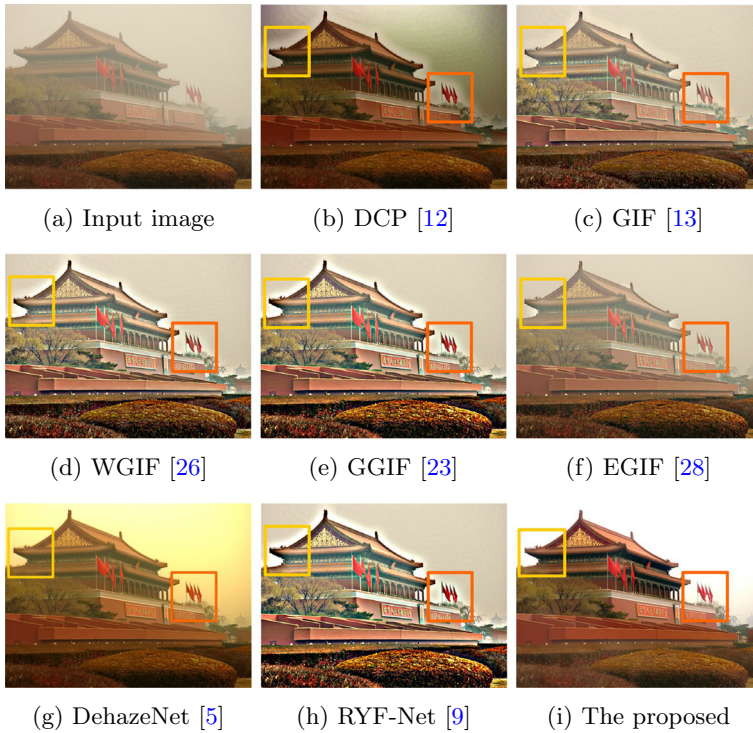(g) DehazeNet [5]   (h) RYF-Net [9]   (i) The proposed

Fig. 5 Dehazed outcomes of different haze removal methods and the proposed method. **a** Input hazy image [1], **b** DCP [12], **c** GIF [13], **d** WGIF [26], **e** GGIF [23], **f** EGIF [28], **g** DehazeNet [5], **h** RYF-Net [9], **i** the proposed

Table 2 Performance comparison on Fattal dataset [10]

Methods	PSNR	SSIM	FADE	CIEDE2000
DCP [12]	17.38	0.7514	2.725	25.57
GIF [13]	19.51	0.7826	2.101	21.16
WGIF [26]	20.08	0.8205	1.686	18.26
GGIF [23]	23.44	0.8519	1.295	15.08
EGIF [28]	27.69	0.8835	0.817	11.55
DehazeNet [5]	27.91	0.8806	0.779	9.68
RYF-Net [9]	29.58	0.9013	0.795	7.93
The proposed	**31.07**	**0.9291**	**0.508**	**5.18**

where $f_{\max}$ is the maximum gray level (255 for 8-bit image). The mean squared error (MSE) measure by the original and the restored image. It is written as

$$\text{MSE} = \frac{1}{m \times n} \sum_{i=0}^{m-1} \sum_{j=0}^{n-1} [f_\text{o}(i, j) - f_\text{r}(i, j)]^2. \tag{36}$$

(a) Input image (b) DCP [12] (c) GIF [13]

(d) WGIF [26] (e) GGIF [23] (f) EGIF [28]

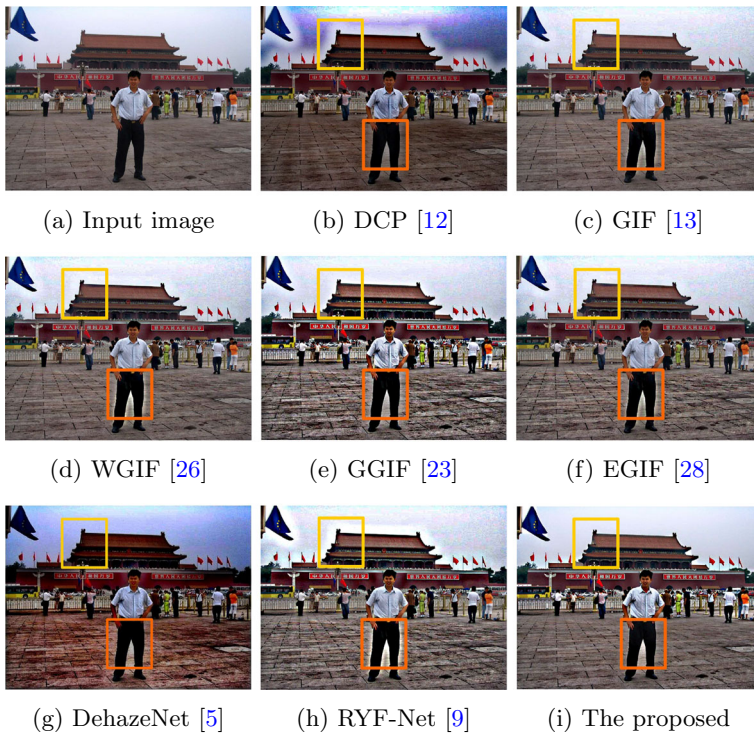(g) DehazeNet [5] (h) RYF-Net [9] (i) The proposed

Fig. 6 Dehazed outcomes of different haze removal methods and the proposed method. **a** Input hazy image [46], **b** DCP [12], **c** GIF [13], **d** WGIF [26], **e** GGIF [23], **f** EGIF [28], **g** DehazeNet [5], **h** RYF-Net [9], **i** the proposed

Table 3 Performance comparison on NYU2 dataset [37]

Methods	PSNR	SSIM	FADE	CIEDE2000
DCP [12]	19.05	0.7794	2.475	23.48
GIF [13]	21.64	0.7906	2.086	20.05
WGIF [26]	22.59	0.8139	1.839	19.17
GGIF [23]	24.77	0.8662	1.416	16.38
EGIF [28]	27.14	0.8791	1.142	12.66
DehazeNet [5]	28.06	0.8838	1.119	10.01
RYF-Net [9]	29.27	0.9171	1.053	8.25
The proposed	**31.69**	**0.9307**	**0.865**	**6.64**

where $m \times n$ represents the size of the image and f_o and f_r are the original and restored images, respectively.

5.2.2 Structural Similarity Index (SSIM)

The structural similarity index (SSIM) [40] metric is used to quantify the structural difference between the source image and recovered image. It has a range $[-1, 1]$ and
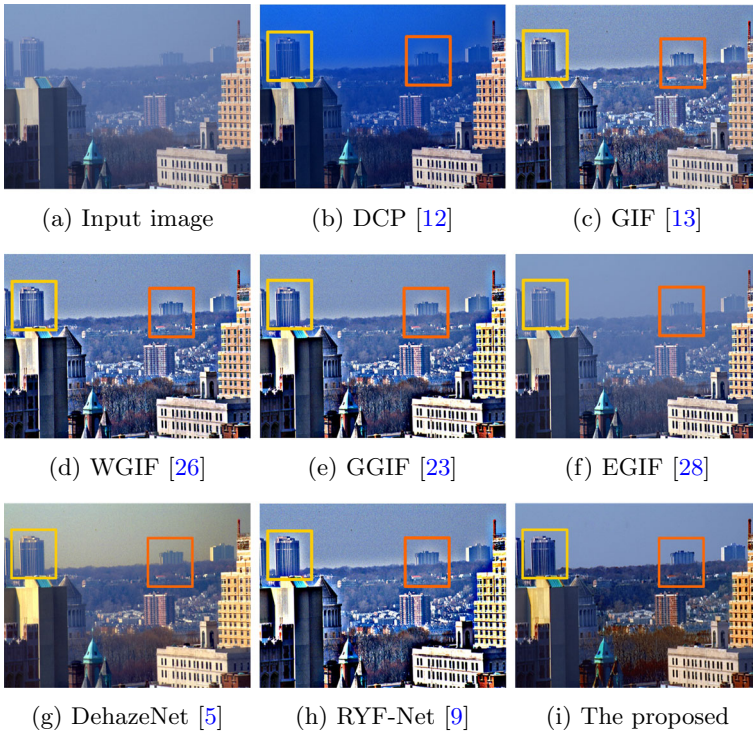
(a) Input image   (b) DCP [12]   (c) GIF [13]

(d) WGIF [26]   (e) GGIF [23]   (f) EGIF [28]

(g) DehazeNet [5]   (h) RYF-Net [9]   (i) The proposed

Fig. 7 Dehazed outcomes of different haze removal methods and the proposed method. **a** Input hazy image [2], **b** DCP [12], **c** GIF [13], **d** WGIF [26], **e** GGIF [23], **f** EGIF [28], **g** DehazeNet [5], **h** RYF-Net [9], **i** the proposed

Table 4 Performance comparison on D-HAZY dataset [1]

Methods	PSNR	SSIM	FADE	CIEDE2000
DCP [12]	22.69	0.8105	2.681	29.07
GIF [13]	23.95	0.8183	2.135	25.49
WGIF [26]	24.72	0.8371	1.861	21.64
GGIF [23]	25.08	0.8509	1.497	18.25
EGIF [28]	27.43	0.8769	1.005	15.31
DehazeNet [5]	28.79	0.8841	1.169	11.97
RYF-Net [9]	**29.88**	**0.9215**	0.985	**7.03**
The proposed	28.15	0.8803	**0.837**	8.11

is expressed as

$$SSIM = F(L_c, C_c, S_c). \tag{37}$$

where L_c, C_c, and S_c represent the luminance, contrast, and saturation comparison, respectively.
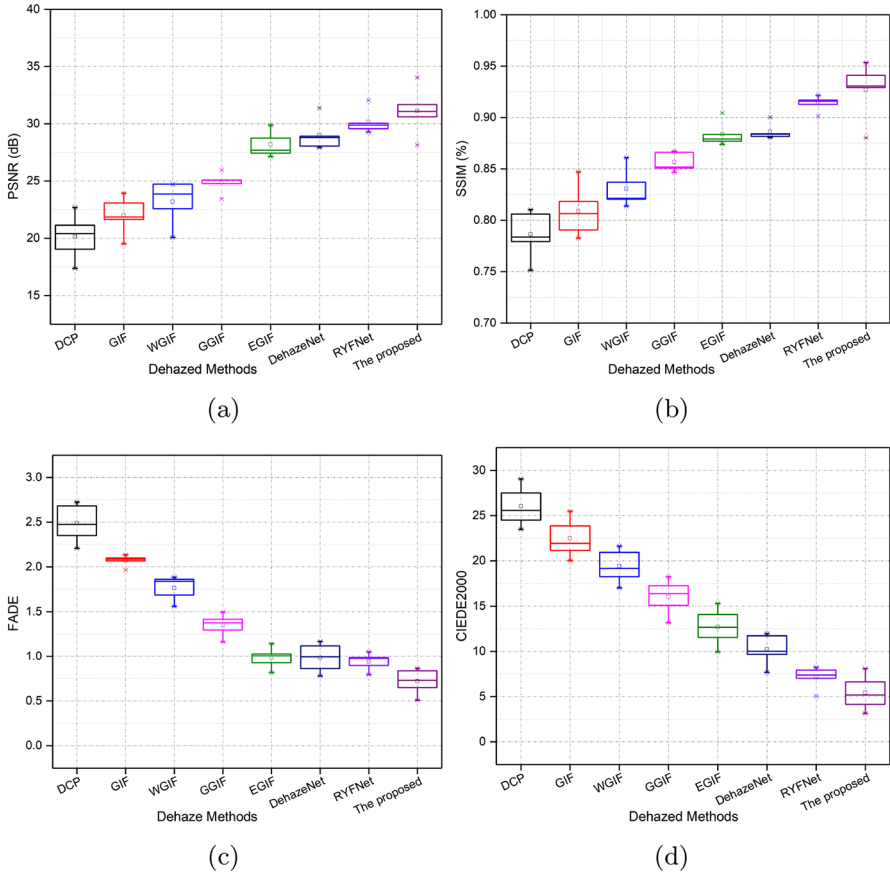
Fig. 8 Box plots [27]-based statistical illustration of different haze removal methods. **a** PSNR [17], **b** SSIM [40], **c** FADE [7], **d** CIEDE2000 [35]

Table 5 Performance comparison on Haze-RD dataset [46]

Methods	PSNR	SSIM	FADE	CIEDE2000
DCP [12]	20.41	0.7837	2.208	27.51
GIF [13]	21.86	0.8065	1.964	23.86
WGIF [26]	24.72	0.8214	1.558	20.94
GGIF [23]	25.08	0.8468	1.163	17.25
EGIF [28]	29.88	0.8739	0.927	14.08
DehazeNet [5]	31.38	0.8815	0.862	11.73
RYF-Net [9]	32.04	0.9128	0.895	7.39
The proposed	**34.05**	**0.9411**	**0.649**	**4.15**

Table 6 Performance comparison on O-HAZE [2]

Methods	PSNR	SSIM	FADE	CIEDE2000
DCP [12]	21.15	0.8059	2.351	24.51
GIF [13]	23.09	0.8471	2.068	21.93
WGIF [26]	23.87	0.8609	1.885	17.02
GGIF [23]	25.96	0.8673	1.375	13.16
EGIF [28]	28.74	0.9045	1.028	9.94
DehazeNet [5]	28.91	0.9004	0.993	7.68
RYF-Net [9]	30.05	0.9159	0.975	5.03
The proposed	**30.61**	**0.9536**	**0.731**	**3.15**

5.2.3 Fog Aware Density Evaluator (FADE)

The fog aware density evaluator (FADE) [7] metric evaluate the perceptual fog density in the restored image. The lower FADE value indicates lower haze concentration.
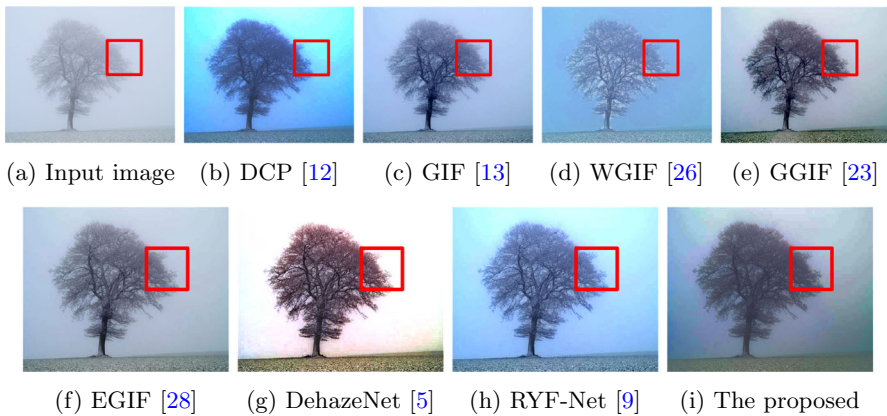
5.2.4 CIEDE2000

The CIEDE2000 metric [35] measures the color fidelity between source image and the dehaze image with ranging [0, 100]. The lower CIEDE2000 value indicates better color correction.

5.3 Discussion

The performance metrics PSNR [17], SSIM [40], FADE [7] and CIEDE2000 [35] of existing DCP [12] GIF [13], WGIF [26], GGIF [23], EGIF [28], DehazeNet [5], RYF-Net [9] and the proposed method are calculated for natural hazy, non-hazy and synthetic images from Fattal [10], NYU2 [37], D-HAZY [1], Haze-RD [46], and O-HAZE [2] datasets. For the best performance, PSNR [17] and SSIM [40] values must be higher, whereas FADE [7] and CIEDE2000 [35] values must be lower. These results are furnished in Tables 2, 3, 4, 5 and 6. The blue bold face values in each row indicate best measured value. PSNR [17] and SSIM [40] values of EGIF [28], DehazeNet [5] and RYF-Net [9] methods are comparable and usually, these values are low for DCP [12] GIF [13], WGIF [26], GGIF [23] methods. Next, RYF-Net [9] is more comparable method which is capable of retaining structures more accurately than the rest of existing methods. FADE [7] and CIEDE2000 [35] values should be small for a better image dehazing. However, these values are higher in DCP [12] GIF [13], WGIF [26], GGIF [23], and EGIF [28] methods. Usually, deep-learning-based DehazeNet [5], and RYF-Net [9] methods produced more comparable FADE [7] values than the existing DCP [12] GIF [13], WGIF [26], GGIF [23], EGIF [28] methods and similar is the case for CIEDE2000 [35] metric scores. It is clear from Tables 2, 3, 4, 5, and 6 that for all the aforesaid datasets the PSNR and SSIM values of the proposed method are higher than the rest of the existing methods, as expected. The FADE values are the least for all the datasets with the proposed method, as expected,

Table 7 Execution time (in sec.)-based assessment

Methods	Fig. 3 250×200	Fig. 4 550×400	Fig. 5 850×600	Fig. 6 1000×950	Fig. 7 1200×1400	Average
DCP [12]	18.27	21.95	26.64	30.55	39.92	27.46
GIF [13]	11.06	16.47	20.19	24.38	32.15	20.85
WGIF [26]	7.34	12.51	18.52	20.09	27.06	17.10
GGIF [23]	4.71	9.62	15.08	17.45	21.54	13.68
EGIF [28]	1.64	6.39	10.91	13.92	18.16	10.20
DehazeNet [5]	1.38	5.05	8.35	10.37	14.39	7.908
RYF-Net [9]	1.15	3.16	4.15	8.09	11.61	5.632
The Proposed	**1.07**	**1.27**	**3.79**	**5.27**	**9.07**	**4.046**

(a) Input image   (b) DCP [12]   (c) GIF [13]   (d) WGIF [26]   (e) GGIF [23]

(f) EGIF [28]   (g) DehazeNet [5]   (h) RYF-Net [9]   (i) The proposed

Fig. 9 Visual outcomes in dense hazy condition

and CIEDE2000 metric values are also the least for Fattal [10], NYU2 [37], Haze-RD [46], and O-HAZE [2] datasets except D-HAZY [1] dataset. This entails that the proposed method is better than the existing dehaze methods. The objective assessment of the performance metrics PSNR [17], SSIM [40], FADE [7], and CIEDE2000 [35] for different existing dehaze methods and the proposed method are computed and tested on images of Fattal [10], NYU2 [37], D-HAZY [1], Haze-RD [46], and O-HAZE [2] datasets. Next, the execution time of DCP [12] GIF [13], WGIF [26], GGIF [23], EGIF [28], DehazeNet [5], RYF-Net [9], and the proposed method for input hazy images in Figs. 3, 4, 5, 6, and 7 having a resolution of 250×200, 550×400, 850×600, 1000×950, and 1400×1200 is calculated and listed in Table 7. It is clear from Table 7 that the proposed method executes, more faster than the fastest reported methods. The statistical analysis of quality metrics PSNR [17], SSIM [40], FADE [7] and CIEDE2000 [35] for DCP [12] GIF [13], WGIF [26], GGIF [23], EGIF [28], DehazeNet [5], RYF-Net [9] and the proposed method represented by a box plot [27] shown in Fig. 8a–d, respectively. It is clear from the box plot figures that the proposed method has a higher median value for PSNR [17] and SSIM [40], whereas lower
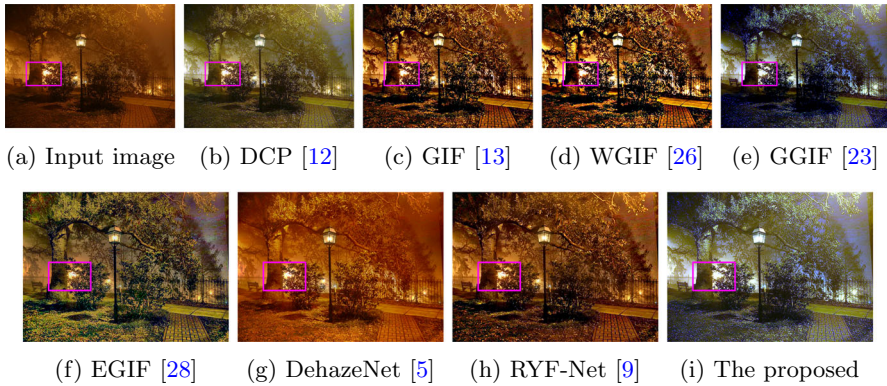
(a) Input image   (b) DCP [12]   (c) GIF [13]   (d) WGIF [26]   (e) GGIF [23]

(f) EGIF [28]   (g) DehazeNet [5]   (h) RYF-Net [9]   (i) The proposed

Fig. 10 Visual outcomes in nighttime hazy condition

median value for FADE [7] and CIEDE2000 [35] metrics in comparison with other existing methods. The horizontal line within the box plot represents median value. Thus, it proves that the proposed method provides better dehaze outcomes than the existing DCP [12] GIF [13], WGIF [26], GGIF [23], EGIF [28], DehazeNet [5], and RYF-Net [9]. Due to limited visibility and poor contrast, the proposed method fails in case of dense haze and nighttime hazy conditions. The failure case of the existing DCP, GIF, WGIF, GGIF, EGIF, DehazeNet, RYF-Net methods and the proposed method on dense haze dataset [3] and nighttime haze dataset [45] is shown in Figs. 9 and 10 respectively. Finally, it is proved from Figs. 2, 3, 4, 5, 6, 7, and 8 and Tables 1, 2, 3, 4, 5, 6, and 7 that the proposed method removes halo artifacts, over-smoothing strongly and preserves edge information more accurately than the existing DCP [12] GIF [13], WGIF [26], GGIF [23], EGIF [28], DehazeNet [5] and RYF-Net [9] methods in both regions. Moreover, the proposed method is fast and preserves edge information in sharp region more accurately compared to the existing haze removal methods.

6 Conclusion

In this paper, an effective scale-aware edge-smoothing weighting constraint-based weighted guided image filter (ESAESWC-WGIF) is proposed to remove haze efficiently. In this filter, a new edge-aware weighting is incorporated into the cost function of the GIF. It refines the initial transmission map more accurately than the existing GIF, WGIF, GGIF, and EGIF methods. It removes halo artifacts, over-smoothing strongly and preserves edge information in both flat and sharp regions. Experimental results prove that the proposed method has better visual quality than the existing methods. About 3,200 images from Fattal, NYU2, D-HAZY, Haze-RD, and O-Haze datasets are used to test the performance of the existing and the proposed dehaze method. We analyzed performance parameters such as PSNR, SSIM, FADE, and CIEDE2000 on these images and experimental results prove that the proposed method restore the images with excellent visual quality. Moreover, the proposed method is independent of the nature of the input image. It performs equally well for all datasets compared to

the existing dehaze methods. It is noteworthy that the proposed method is faster than the existing methods for a given resolution of images. But, this method fails in case of dense hazy and nighttime hazy conditions. The failure results in dense hazy and nighttime hazy conditions are shown in Figs. 9 and 10, respectively. So, there is a scope to devise a new method which can satisfy these requirements. We will be exploring the suitability of the proposed method for wider applications such as satellite image, underwater image, and low-light images dehazing.

Data Availability The datasets generated or analyzed during the present study are available from the corresponding author upon reasonable request.

References

1. C. Ancuti, C.O. Ancuti, C. De Vleeschouwer, D-HAZY: a dataset to evaluate quantitatively dehazing algorithms. In *2016 IEEE International Conference on Image Processing (ICIP)*, pp. 2226–2230. IEEE (2016). https://doi.org/10.1109/ICIP.2016.7532754
2. C.O. Ancuti, C. Ancuti, R. Timofte, C. De Vleeschouwer, O-HAZE: a dehazing benchmark with real hazy and haze-free outdoor images. In *2018 IEEE/CVF Conference on Computer Vision and Pattern Recognition Workshops (CVPRW)*, pp. 867–8678 (2018). https://doi.org/10.1109/CVPRW.2018.00119
3. C.O. Ancuti, C. Ancuti, M. Sbert, R. Timofte, Dense-Haze: a benchmark for image dehazing with dense-haze and haze-free images. In *2019 IEEE International Conference on Image Processing (ICIP)*, pp. 1014–1018 (2019). https://doi.org/10.1109/ICIP.2019.8803046
4. T.M. Bui, W. Kim, Single image dehazing using color ellipsoid prior. IEEE Trans. Image Process. **27**(2), 999–1009 (2017). https://doi.org/10.1109/TIP.2017.2771158
5. B. Cai, X. Xu, K. Jia, C. Qing, D. Tao, DehazeNet: an end-to-end system for single image haze removal. IEEE Trans. Image Process. **25**(11), 5187–5198 (2016). https://doi.org/10.1109/TIP.2016.2598681
6. B. Chen, S. Wu, Weighted aggregation for guided image filtering. Signal Image Video Process. **14**(3), 491–498 (2020). https://doi.org/10.1007/s11760-019-01579-1
7. L.K. Choi, J. You, A.C. Bovik, Referenceless prediction of perceptual fog density and perceptual image defogging. IEEE Trans. Image Process. **24**(11), 3888–3901 (2015). https://doi.org/10.1109/TIP.2015.2456502
8. N.R. Draper, H. Smith, *Applied Regression Analysis*, vol. 326 (Wiley, New York, 1998)
9. A. Dudhane, S. Murala, RYF-Net: deep fusion network for single image haze removal. IEEE Trans. Image Process. **29**, 628–640 (2020). https://doi.org/10.1109/TIP.2019.2934360
10. R. Fattal, Single image dehazing. ACM Trans. Graph. (TOG) **27**(3), 1–9 (2008). https://doi.org/10.1145/1360612.1360671
11. H. Geethu, S. Shamna, J.J. Kizhakkethottam, Weighted guided image filtering and haze removal in single image. Procedia Technol. **24**, 1475–1482 (2016). https://doi.org/10.1016/j.protcy.2016.05.248
12. K. He, J. Sun, X. Tang, Single image haze removal using dark channel prior. IEEE Trans. Pattern Anal. Mach. Intell. **33**(12), 2341–2353 (2010). https://doi.org/10.1109/TPAMI.2010.168
13. K. He, J. Sun, X. Tang, Guided image filtering. IEEE Trans. Pattern Anal. Mach. Intell. **35**(6), 1397–1409 (2012). https://doi.org/10.1109/TPAMI.2012.213
14. L. He, J. Zhao, N. Zheng, D. Bi, Haze removal using the difference–structure–preservation prior. IEEE Trans. Image Process. **26**(3), 1063–1075 (2016). https://doi.org/10.1109/TIP.2016.2644267
15. G.-S. Hong, B.-G. Kim, A local stereo matching algorithm based on weighted guided image filtering for improving the generation of depth range images. Displays **49**, 80–87 (2017). https://doi.org/10.1016/j.displa.2017.07.006
16. G.-S. Hong, J.-K. Park, B.-G. Kim, Near real-time local stereo matching algorithm based on fast guided image filtering. In *2016 6th European Workshop on Visual Information Processing (EUVIP)*, pp. 1–5. IEEE (2016). https://doi.org/10.1109/EUVIP.2016.7764595
17. Q. Huynh-Thu, M. Ghanbari, Scope of validity of PSNR in image/video quality assessment. Electron. Lett. **44**(13), 800–801 (2008). https://doi.org/10.1049/el:20080522

18. H. Israël, F. Kasten, Koschmieders theorie der horizontalen sichtweite. In *Die Sichtweite im Nebel und die Möglichkeiten ihrer künstlichen Beeinflussung*, pp. 7–10. Springer (1959). https://doi.org/10.1007/978-3-663-04661-5_2

19. M. Ju, C. Ding, D. Zhang, Y.J. Guo, BDPK: Bayesian dehazing using prior knowledge. IEEE Trans. Circuits Syst. Video Technol. **29**(8), 2349–2362 (2018). https://doi.org/10.1109/TCSVT.2018.2869594

20. M. Ju, C. Ding, Y.J. Guo, D. Zhang, IDGCP: image dehazing based on Gamma correction prior. IEEE Trans. Image Process. **29**, 3104–3118 (2019). https://doi.org/10.1109/TIP.2019.2957852

21. M. Ju, C. Ding, W. Ren, Y. Yang, IDBP: image dehazing using blended priors including non-local, local, and global priors. IEEE Trans. Circuits Syst. Video Technol. (2021). https://doi.org/10.1109/TCSVT.2021.3101503

22. J. Kopf, B. Neubert, B. Chen, M. Cohen, D. Cohen-Or, O. Deussen, M. Uyttendaele, D. Lischinski, Deep photo: model-based photograph enhancement and viewing. ACM Trans. Graph. (TOG) **27**(5), 1–10 (2008). https://doi.org/10.1145/1409060.1409069

23. F. Kou, W. Chen, C. Wen, Z. Li, Gradient domain guided image filtering. IEEE Trans. Image Process. **24**(11), 4528–4539 (2015). https://doi.org/10.1109/TIP.2015.2468183

24. B. Li, X. Peng, Z. Wang, J. Xu, D. Feng, AOD-Net: All-in-one dehazing network. In *2017 IEEE International Conference on Computer Vision (ICCV)*, pp. 4780–4788 (2017). https://doi.org/10.1109/ICCV.2017.511

25. C. Li, C. Guo, J. Guo, P. Han, H. Fu, R. Cong, PDR-Net: perception-inspired single image dehazing network with refinement. IEEE Trans. Multimed. **22**(3), 704–716 (2019). https://doi.org/10.1109/TMM.2019.2933334

26. Z. Li, J. Zheng, Z. Zhu, W. Yao, S. Wu, Weighted guided image filtering. IEEE Trans. Image process. **24**(1), 120–129 (2014). https://doi.org/10.1109/TIP.2014.2371234

27. S. Lin, C. Wong, G. Jiang, M. Rahman, T. Ren, N. Kwok, H. Shi, Y.-H. Yu, T. Wu, Intensity and edge based adaptive unsharp masking filter for color image enhancement. Optik **127**(1), 407–414 (2016). https://doi.org/10.1016/j.ijleo.2015.08.046

28. Z. Lu, B. Long, K. Li, F. Lu, Effective guided image filtering for contrast enhancement. IEEE Signal Process. Lett. **25**(10), 1585–1589 (2018). https://doi.org/10.1109/LSP.2018.2867896

29. Z. Lu, B. Long, S. Yang, Saturation based iterative approach for single image dehazing. IEEE Signal Process. Lett. **27**, 665–669 (2020). https://doi.org/10.1109/LSP.2020.2985570

30. E.J. McCartney, *Optics of the Atmosphere: Scattering by Molecules and Particles* (Wiley, New York, 1976)

31. A.K. Moorthy, A.C. Bovik, A two-step framework for constructing blind image quality indices. IEEE Signal Process. Lett. **17**(5), 513–516 (2010). https://doi.org/10.1109/LSP.2010.2043888

32. S.G. Narasimhan, S.K. Nayar, Chromatic framework for vision in bad weather. In *Proceedings IEEE Conference on Computer Vision and Pattern Recognition*. CVPR 2000 (Cat. No. PR00662), volume 1, pp. 598–605. IEEE (2000). https://doi.org/10.1109/CVPR.2000.855874

33. S.G. Narasimhan, S.K. Nayar, Vision and the atmosphere. Int. J. Comput. Vis. **48**(3), 233–254 (2002). https://doi.org/10.1023/A:1016328200723

34. X. Qin, Z. Wang, Y. Bai, X. Xie, H. Jia, FFA-Net: feature fusion attention network for single image dehazing. In *Proceedings of the AAAI Conference on Artificial Intelligence*, vol. 34, pp. 11908–11915 (2020). https://doi.org/10.1609/aaai.v34i07.6865

35. G. Sharma, W. Wu, E.N. Dalal, The CIEDE2000 color-difference formula: implementation notes, supplementary test data, and mathematical observations. Color Res. Appl. **30**(1), 21–30 (2005). https://doi.org/10.1002/col.20070

36. S. Shwartz, E. Namer, Y.Y. Schechner, Blind haze separation. In *2006 IEEE Computer Society Conference on Computer Vision and Pattern Recognition (CVPR'06)*, volume 2, pp. 1984–1991. IEEE (2006). https://doi.org/10.1109/CVPR.2006.71

37. N. Silberman, D. Hoiem, P. Kohli, R. Fergus, Indoor segmentation and support inference from rgbd images. In *European Conference on Computer Vision*, pp. 746–760. Springer (2012). https://doi.org/10.1007/978-3-642-33715-4_54

38. R.T. Tan, Visibility in bad weather from a single image. In *2008 IEEE Conference on Computer Vision and Pattern Recognition*, pp. 1–8. IEEE (2008). https://doi.org/10.1109/CVPR.2008.4587643

39. C. Tomasi, R. Manduchi, Bilateral filtering for gray and color images. In *Sixth International Conference on Computer Vision*, pp. 839–846. IEEE (1998). https://doi.org/10.1109/ICCV.1998.710815

40. Z. Wang, A.C. Bovik, H.R. Sheikh, E.P. Simoncelli, Image quality assessment: from error visibility to structural similarity. IEEE Trans. Image Process. **13**(4), 600–612 (2004). https://doi.org/10.1109/TIP.2003.819861

41. S.K. Yadav, K. Sarawadekar, Single image dehazing using adaptive gamma correction method. In *TENCON 2019: 2019 IEEE Region 10 Conference (TENCON)*, pp. 1752–1757. IEEE (2019). https://doi.org/10.1109/TENCON.2019.8929383

42. S.K. Yadav, K. Sarawadekar, Steering kernel-based guided image filter for single image dehazing. In *2020 IEEE Region 10 Conference (TENCON)*, pp. 444–449. IEEE (2020). https://doi.org/10.1109/TENCON50793.2020.9293825

43. D. Yang, J. Sun, Proximal Dehaze-Net: a prior learning-based deep network for single image dehazing. In *Proceedings of the European Conference on Computer Vision (ECCV)*, pp. 729–746 (2018). https://doi.org/10.1007/978-3-030-01234-2_43

44. B. Zhang, J.P. Allebach, Adaptive bilateral filter for sharpness enhancement and noise removal. IEEE Trans. Image Process. **17**(5), 664–678 (2008). https://doi.org/10.1109/TIP.2008.919949

45. J. Zhang, Y. Cao, S. Fang, Y. Kang, C.W. Chen, Fast haze removal for nighttime image using maximum reflectance prior. In *2017 IEEE Conference on Computer Vision and Pattern Recognition (CVPR)*, pp. 7016–7024 (2017). https://doi.org/10.1109/CVPR.2017.742

46. Y. Zhang, L. Ding, G. Sharma, HazeRD: an outdoor scene dataset and benchmark for single image dehazing. In *2017 IEEE International Conference on Image Processing (ICIP)*, pp. 3205–3209. IEEE (2017). https://doi.org/10.1109/ICIP.2017.8296874

47. S. Zhao, L. Zhang, Y. Shen, Y. Zhou, RefineDNet: a weakly supervised refinement framework for single image dehazing. IEEE Trans. Image Process. **30**, 3391–3404 (2021). https://doi.org/10.1109/TIP.2021.3060873

48. Q. Zhu, J. Mai, L. Shao, A fast single image haze removal algorithm using color attenuation prior. IEEE Trans. Image Process. **24**(11), 3522–3533 (2015). https://doi.org/10.1109/TIP.2015.2446191

49. E.R. Ziegel, The elements of statistical learning. Technometrics **45**(3), 267–268 (2003). https://doi.org/10.1198/tech.2003.s770